Radiology

Diffusion-weighted MR Imaging in Laryngeal and Hypopharyngeal Carcinoma: Association between Apparent Diffusion Coefficient and Histologic Findings[1]

Juliette P. Driessen, MD
Joana Caldas-Magalhaes
Luuk M. Janssen, MD, PhD
Frank A. Pameijer, MD, PhD
Nina Kooij, MD
Chris H. J. Terhaard, MD, PhD
Wilko Grolman, MD, PhD
Marielle E. P. Philippens, MD, PhD

Purpose: To investigate the relationship between the histologic characteristics of head and neck squamous cell carcinoma and apparent diffusion coefficient (ADC) at diffusion-weighted magnetic resonance (MR) imaging.

Materials and Methods: The institutional ethics committee approved this study and waived informed consent. In head and neck squamous cell carcinoma, local failure after chemotherapy and/or radiation therapy correlates with pretreatment ADC. However, the histopathologic basis of this correlation remains unclear. In this study, 16 patients with head and neck squamous cell carcinoma were enrolled (median age, 60 years; range, 49–78 years). Before undergoing total laryngectomy, patients underwent 1.5-T diffusion-weighted MR imaging. After resection, whole-mount hematoxylin-eosin–stained sections were registered to the MR images. Cellular density; nuclear, cytoplasmic, and stromal area; and nuclear-cytoplasmic ratio within the tumor were calculated by using image-based segmentation on four consecutive slices. Mean ADC of the corresponding tumor region was calculated. Spearman correlations between ADC and histologic characteristics were calculated.

Results: ADC was significantly and inversely correlated with cell density ($n = 16$, $r = -0.57$, $P = .02$), nuclear area ($n = 12$, $r = -0.64$, $P = .03$), and nuclear-cytoplasmic ratio ($n = 12$, $r = -0.77$, $P \leq .01$). ADC was significantly and positively correlated with percentage area of stroma ($n = 12$, $r = 0.69$, $P = .01$). Additionally, the percentage area of stroma was strongly interdependent with the percentage area of nuclei ($n = 12$, $r = -0.97$, $P \leq .01$).

Conclusion: ADC was significantly correlated with cellularity, stromal component, and nuclear-cytoplasmic ratio. The positive correlation of ADC and stromal component suggests that the poor prognostic value of high pretreatment ADC might partly be attributed to the tumor-stroma component, a known predictor of local failure.

[1] From the Department of Otorhinolaryngology–Head and Neck Surgery (J.P.D., L.M.J., W.G.), Rudolf Magnus Institute of Neuroscience (J.P.D., W.G.), Department of Radiotherapy (J.C.M., C.H.J.T., M.E.P.P.), Department of Radiology (F.A.P.), and Department of Pathology (N.K.), University Medical Center Utrecht, hp G05.129, Heidelberglaan 100, 3584 CX Utrecht, the Netherlands. Received May 22, 2013; revision requested July 12; revision received January 12, 2014; accepted February 3; final version accepted February 25. **Address correspondence to** J.P.D. (e-mail: *j.p.driessen-3@umcutrecht.nl*).

In head and neck squamous cell carcinomas, magnetic resonance (MR) imaging is increasingly used because it provides excellent soft-tissue contrast in this complex and heterogeneous region. Besides conventional anatomic images, there is a rising trend toward additional functional MR imaging, such as diffusion-weighted imaging (DWI), for further characterization of tissues (1). DWI is an established imaging technique in the early detection of acute stroke, and it is gaining increasing importance in several oncologic applications (2). DWI is used to quantify the diffusional motion of water with the apparent diffusion coefficient (ADC). As such, the ADC provides information about the microenvironment of tissues (3,4). DWI has proven to be highly accurate in the differentiation of benign from malignant lesions, and it can be used for tissue characterization of primary tumors and metastasis (5–7). DWI seems particularly promising in the prediction of tumor radiosensitivity and the early assessment of treatment response, since high pretreatment ADC has been shown to be correlated with local failure of chemotherapy and/or radiation therapy and might therefore become an important application for treatment personalization (8–13).

A number of variables are presumed to influence the mobility of water protons. Commonly, the restriction of water molecules in tumors is attributed to increased cellular density (CD) and decreased interstitial space (14–16). However, perfusion, tortuosity of the extracellular space, and integrity of cellular membranes affect diffusivity. In prostate tissue and central nervous system lymphomas, an inverse correlation between ADC and CD has been found (15–18). However, limited studies have been conducted to investigate the relationship between ADC and other microanatomic features, and the histopathologic basis of the association between high ADC and local failure remains unclear (19,20).

The aim of this study was to investigate the relationship between histologic characteristics of head and neck squamous cell carcinoma and ADC.

Advances in Knowledge

- Apparent diffusion coefficient (ADC) was positively related to the percentage area of stroma ($r = 0.69$, $P = .01$).
- ADC was negatively related to the absolute number of cells per square millimeter ($r = -0.57$, $P = .02$), the percentage area of nuclei ($r = -0.64$, $P = .03$), and the nuclear-cytoplasmic ratio ($r = -0.77$, $P \leq .01$).

Implications for Patient Care

- Pretreatment ADC and corresponding microanatomic parameters are related, which may improve the interpretation of diffusion-weighted MR images.
- The reported poor prognostic value of high pretreatment ADC in head and neck squamous cell carcinoma might be explained by the corresponding high stromal content of the tumor.

Materials and Methods

Patients

The institutional ethics committee approved this study and waived informed consent. Eighteen consecutive patients were enrolled between June 2009 and April 2011 as part of an ongoing study, and all data were reviewed retrospectively. Inclusion criteria were biopsy-proven laryngeal or hypopharyngeal squamous cell carcinoma without prior treatment, stage T3 or T4 disease, and planned curative total laryngectomy with or without partial pharyngectomy. Before surgery, patients underwent a 1.5-T MR imaging examination that included DWI. Two patients were excluded from analysis, owing to failure of the histologic section preparation ($n = 1$) or incomplete DWI protocol ($n = 1$). Sixteen patients remained for analysis. Eight patients (50%) were included in our previous publication on the development of the registration method for the imaging validation study by Caldas-Magalhaes et al (21).

MR Imaging Protocol

Before undergoing surgery, all patients underwent MR imaging performed with a 1.5-T MR imaging system (Intera; Philips Medical Systems) with a small, two-element flexible surface receiver coil. MR sequences included T1-weighted imaging before and after administration of gadolinium-based contrast agent (repetition time msec/echo time msec, 593/15) and T2-weighted (4200/130) imaging. DWI images were obtained by using a multisection single-shot spin-echo echo-planar imaging sequence, with short inversion time inversion-recovery fat suppression (5872/70, inversion time of 180 msec, four signals acquired, field of view of 25 × 20 cm^2, section thickness of 4 mm, acquisition matrix of 121 × 101 mm^2, intersection gap of 0 mm, and b values of 0, 150, and 800 sec/mm^2). ADC values were calculated with b values of 150 and 800 sec/mm^2. The median time interval between MR imaging and surgery was 9 days (range, 1–34 days).

Whole-Mount Histologic Section Preparation

Histologic section preparation and imaging registration were described previously (21). Briefly, the following steps were performed. After surgery,

Published online before print
10.1148/radiol.14131173 **Content codes:** HN MR

Radiology 2014; 272:456–463

Abbreviations:
ADC = apparent diffusion coefficient
CD = cellular density
DWI = diffusion-weighted imaging
H-E = hematoxylin-eosin
NC = nuclear-cytoplasmic

Author contributions:
Guarantors of integrity of entire study, J.P.D., L.M.J., F.A.P., N.K., C.H.J.T., M.E.P.P.; study concepts/study design or data acquisition or data analysis/interpretation, all authors; manuscript drafting or manuscript revision for important intellectual content, all authors; approval of final version of submitted manuscript, all authors; literature research, J.P.D., L.M.J., C.H.J.T., M.E.P.P.; clinical studies, J.P.D., J.C.M., L.M.J., F.A.P., C.H.J.T., W.G., M.E.P.P.; experimental studies, J.P.D., J.C.M., L.M.J., C.H.J.T.; statistical analysis, J.P.D., J.C.M., L.M.J., C.H.J.T.; and manuscript editing, all authors

Conflicts of interest are listed at the end of this article.

the fresh surgical specimen was fixed in 10% formaldehyde for at least 48 hours. After fixation, computed tomography of the specimen was performed. Subsequently, to prevent deformations during the slicing procedure, the specimen was solidified in 5% agarose before it was sliced in 3-mm-thick slices and photographed. Special attention was paid to the orientation of the specimen in the agarose block, so that the slice direction was comparable to the presurgical images. Finally, after removal of the agarose and decalcification, 4-μm whole-mount microscopic slices were cut from the macroscopic slices and stained with hematoxylin-eosin (H-E) with standard histologic procedure. Cross-sectional area of the tumor was outlined on the H-E sections by an experienced pathologist (N.K., with 6 years of experience).

Registration of MR Images and Pathologic Specimens

The MR images were registered semiautomatically to the H-E sections as described previously (21). Briefly, each H-E section was first registered to the corresponding photographed macroscopic slice. Second, a three-dimensional specimen was reconstructed from the stacked photographs of the macroscopic slices, and, finally, the reconstructed three-dimensional specimen was registered to the T1-weighted MR images after gadolinium-based contrast material administration by using the outlining of the thyroid and cricoid cartilage as a reference. The DWI MR sections were registered by using the same transformation as that used for the T1-weighted MR images. This method provides a highly accurate three-dimensional registration, with a mean error of 3 mm in the axial plane owing to registration errors and specimen deformation (21).

Selection of Regions of Interest

Four consecutive microscopic slides per patient, containing the largest tumor diameter, were chosen for further analysis and digitized at histologic resolution (objective magnification, ×20) (ScanScope XT bright-field scanner; Aperio Technologies, Vista, Calif). The corresponding level of DWI sections was identified by using the three-dimensional registration. DWI sections have geometric distortions compared with native MR images, but only in the phase-encoded direction (anterior-posterior direction). Therefore, we could not transfer the delineation of the pathologist directly from the H-E sections to the DWI sections. The tumor was thus manually delineated on images with a b value of 0 sec/mm^2 by using the additional information from all other MR images by two physicians in consensus, independent of the delineation of the pathologist (J.P.D., a resident otorhinolaryngologist with 2 years of experience in DWI; and F.A.P., a radiologist with more than 15 years of experience in head and neck radiology). Figure 1 shows an H-E section, including the pathologists' delineation, registered to the MR images and the manual delineation of the DWI on the corresponding level.

Figure 1

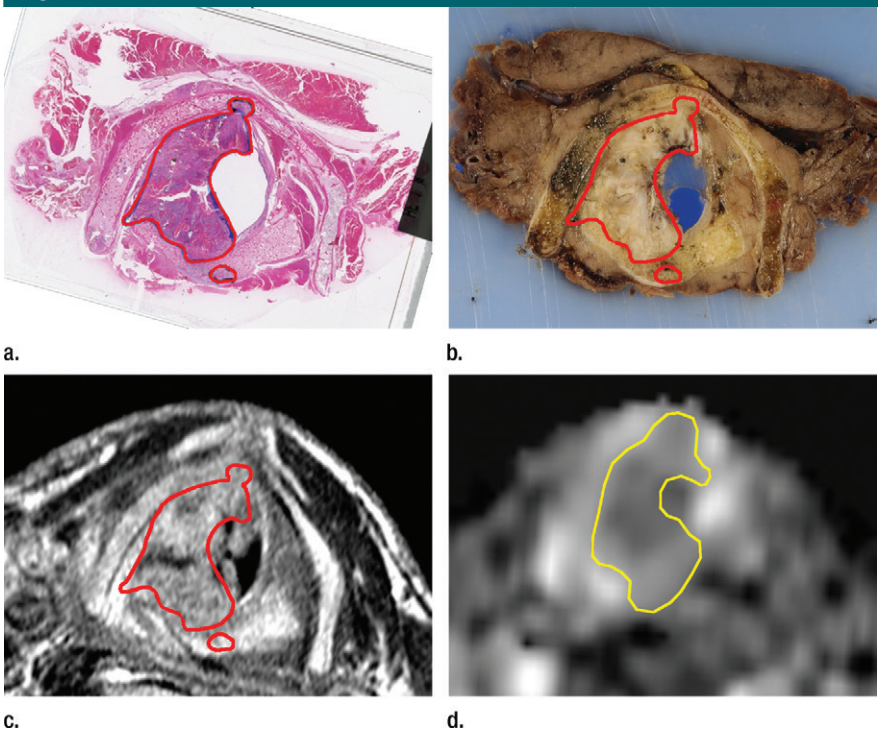

Figure 1: Images show DWI sections registered with pathologic and histologic specimens from a 78-year-old man with a T3 glottic laryngeal carcinoma. The tumor is depicted in **(a)** the whole-mount digitized H-E section, **(b)** the corresponding macroscopic slice of the specimen, **(c)** the axial registered T1-weighted MR image acquired after injection of gadolinium-based contrast material, and **(d)** the ADC map. The delineation made by the pathologist on the H-E section (red outlines on **a**) was transferred to the MR image with an error of less than 3 mm to ensure the corresponding level of the DWI. A manual delineation was made on the DWI (b = 0 mm/sec^2) section on the corresponding level, and ADC values were calculated (yellow outline on **d**).

Microanatomic Parameters from H-E Sections

Microanatomic analysis was performed on the cross-sectional tumor area, delineated by the pathologist on the four selected consecutive H-E sections per patient. The absolute number of cell nuclei (the CD) within the tumor was identified by using the IHC Nuclear Algorithm v8 in ImageScope v10.0 (Aperio Technologies) in the region delineated by the pathologist. The nuclear algorithm is based on color, size, shape, and surroundings

Table 1

Patient Characteristics

Characteristic	Value
Age (y)*	60 (49–78)
Tumor site	
Supraglottic	6 (38)
Glottis	2 (13)
Transglottic	3 (18)
Piriform sinus	5 (31)
Pathologic tumor stage	
T3	3 (18)
T4a	12 (75)
T4b	1 (6)
Differentiation	
Moderate	9 (56)
Poor	7 (44)
Interval between MR imaging and surgery (d)*	9 (1–34)

Note.—Unless specified otherwise, data are numbers of patients, with percentages in parentheses.

* Data are median values, with ranges in parentheses.

and was designed with a minimal detectable nuclear size of 20 μm^2 (22). This algorithm was validated by manually counting the CD in a random area of 800 μm^2 within the tumor on the most cranial chosen H-E section. Bland-Altman analysis showed a mean bias ± standard deviation of 9.6% ± 11.4.

The ratios of cellular components were identified by using color-based segmentation with the Positive Pixel Count Algorithm v9 in ImageScope (Aperio Technologies). The percentage area of nuclei, cytoplasm, and stroma was calculated by using two hue and window settings (setting 1: 0.10 for hue, 0.44 for window; setting 2: 0.72 for hue, 0.36 for window).

The area of each component was calculated as the ratio of the segmented area to the area of the tumor delineated by the pathologist. The area of nuclei was segmented as negative pixels in setting 1. Stroma was segmented as negative pixels in setting 2. Cytoplasm and nuclei were segmented as positive in setting 2; therefore, the percentage area of cytoplasm was the subtraction of the area of cytoplasm plus nuclei (positive setting 2) minus the area of nuclei (negative setting 1) (19). Finally, the nuclear-cytoplasmic (NC) ratio was calculated.

Statistical Analysis

For each tumor, median ADC, CD, and proportion of cellular components were calculated. Spearman correlation coefficients were calculated. The Student *t* test was used to test the difference between ADC values in different histologic tumor grades. Two-tailed *P* values of up to .05 were considered to indicate a significant difference. For the correlation of simultaneously tested hypotheses (percentage area of nuclei, stroma, and cytoplasm and the NC ratio), the Holm-Bonferroni adjustment for multiple comparisons was used (GraphPad Prism 6; GraphPad, La Jolla, Calif).

Results

Sixteen patients were eligible for analysis of the CD. For the analyses of the cellular components with a color-based segmentation method, 12 patients were eligible, as four patients were excluded because poor staining intensity hindered reliable separation of cytoplasm and nuclei. Patients' clinical characteristics are summarized in Table 1.

Figure 2 shows a typical example of the automatic segmentation on the H-E sections.

The mean ADC of tumors showed wide variation, with a range of (0.92–1.30) × 10^{-3} mm^2/sec. ADC heterogeneity also varied widely among tumors, with a standard deviation range of (0.15–0.34) × 10^{-3} mm^2/sec. Table 2 displays the mean values of the microanatomic parameters and the Spearman correlations with ADC and with each other. ADC was significantly and inversely correlated to the CD, the nuclear area, and the NC ratio. ADC was significantly and positively correlated with the stromal area (Fig 3). No significant correlation was found between ADC and cytoplasmic area.

Additionally, nuclear and stromal areas were very strongly and inversely correlated. This correlation shows their interdependence, although they result from different algorithm settings.

Figures 4–6 show examples of three tumors with different tissue microanatomy, the corresponding CD, ratios of cellular components, and ADC values.

All tumors showed less than 5% necrosis (range, 1%–5%), and moderately differentiated tumors showed no difference in ADC compared with poorly differentiated tumors ([1.13 vs 1.05] × 10^{-3} mm^2/sec; P = .20).

Discussion

Exploration of the relationship between tissue microanatomy and ADC is of great importance to improve interpretation of DWI findings and clarify the predictive value of ADC in treatment response.

In this study, we found a significant and inverse correlation between ADC and CD of moderate strength. Nuclear area and the NC ratio showed moderate to strong inverse correlation with ADC, and stromal area showed a moderate to strong positive correlation. Additionally, nuclear and stromal area showed strong interdependence.

The inverse correlation between ADC and CD reinforces the model that higher cellularity, with cells packed more densely, causes restriction of water diffusion. This inverse correlation has been reported previously in prostate cancer and lymphomas (15–18). However, previous reports were limited to the percentage area of nuclei solely. Although the percentage area of nuclei is partly determined by the absolute number of cells, it is also influenced by the size of the nuclei, whereas CD is independent of nuclear size. The correlation between ADC and CD has been investigated previously by Barajas et al in central nervous system lymphomas by means of manual cell count from a core biopsy sample (15). In that study, however, no registration was performed between pathologic specimens and imaging. Therefore, accurate location of the biopsy within the tumor was not taken into account. In squamous cell carcinomas of the head and neck, which are known for their heterogeneity, this

Figure 2

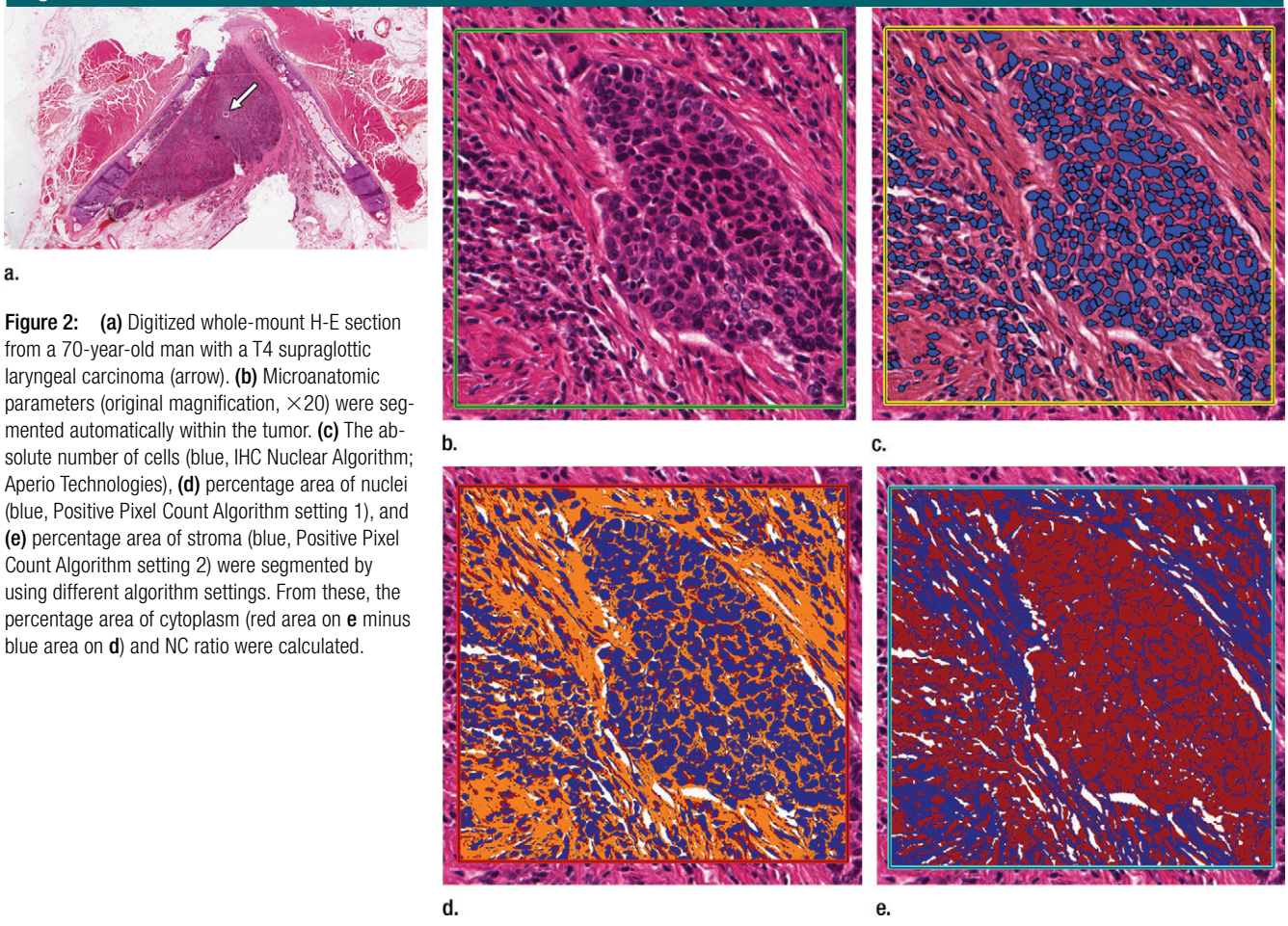

Figure 2: **(a)** Digitized whole-mount H-E section from a 70-year-old man with a T4 supraglottic laryngeal carcinoma (arrow). **(b)** Microanatomic parameters (original magnification, ×20) were segmented automatically within the tumor. **(c)** The absolute number of cells (blue, IHC Nuclear Algorithm; Aperio Technologies), **(d)** percentage area of nuclei (blue, Positive Pixel Count Algorithm setting 1), and **(e)** percentage area of stroma (blue, Positive Pixel Count Algorithm setting 2) were segmented by using different algorithm settings. From these, the percentage area of cytoplasm (red area on **e** minus blue area on **d**) and NC ratio were calculated.

Table 2

Microanatomic Parameters and Correlation with ADC

Parameter	CD ($n = 16$)	Percentage Nuclei Area ($n = 12$)	Percentage Cytoplasm Area ($n = 12$)	Percentage Stroma Area ($n = 12$)	NC Ratio ($n = 12$)
Mean*	6406 (4806–8050)	43.1 (24.1–70.2)	19.6 (11.2–27.1)	39.6 (14.0–75.8)	2.4 (1.1–4.7)
Correlation with ADC (r value)†	−0.57 (.02‡)	−0.64 (.03§)	0.43 (.16)	0.69 (.01§)	−0.77 (< .01§)
Correlation with percentage nuclei (r value)†	…	1.000	−0.01 (.97)	−0.97 (<.01‡)	0.64 (.03‡)

Note.—CD = absolute number of cells per square millimeter, r = Spearman ρ.

* Unless specified otherwise, data are mean values, with ranges in parentheses.

† Numbers in parentheses are P values.

‡ Significant difference.

§ Significant difference by using Holm-Bonferroni adjustment for multiple testing.

method would be inappropriate. Instead, in our study, we used four consecutive whole-mount histologic sections, registered to MR images with a highly accurate and validated registration technique (21). This method had a mean error of only 3 mm.

In contrast to prior literature, our study extended beyond tissue cellularity by including the investigation of numerous other tissue components. We found a moderate to strong significantly positive correlation of ADC and stromal area. Stromal area generally has more extracellular volume compared with a

Figure 3

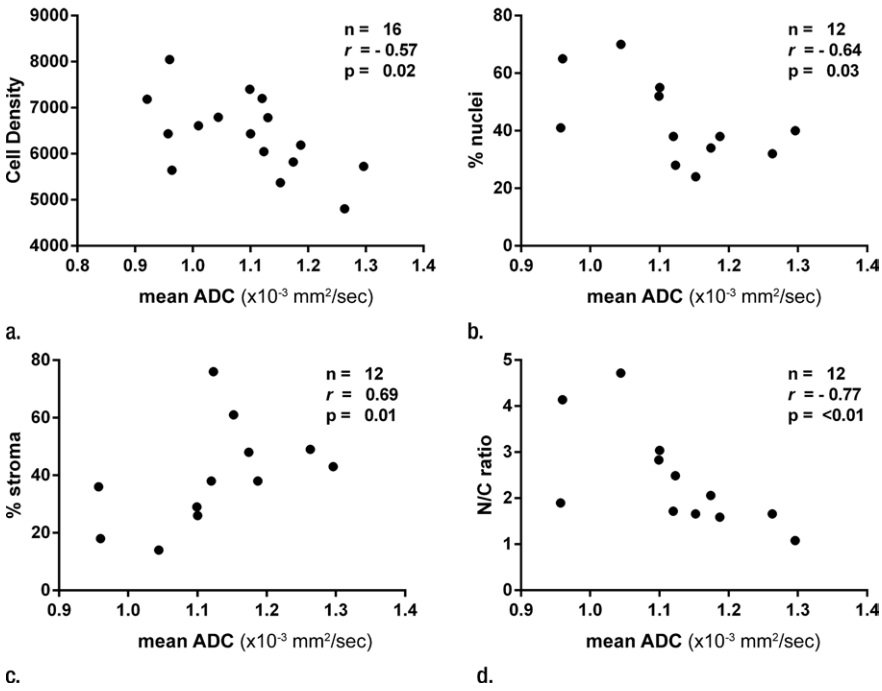

Figure 3: Plots show the correlation of mean ADC with **(a)** CD, **(b)** nuclear area, **(c)** stromal area, and **(d)** NC *(N/C)* ratio. Correlations were calculated with a nonparametric test. *r* = Spearman ρ statistic.

Figure 4

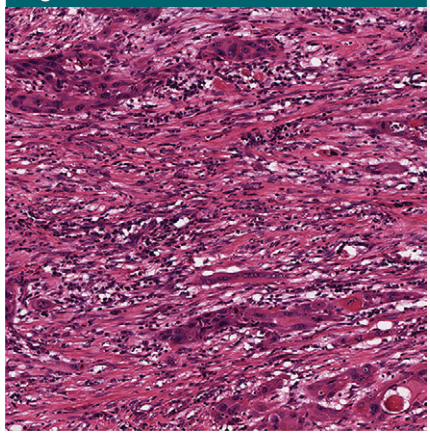

Figure 4: Digitized whole-mount H-E section (original magnification, ×10) of a T4a laryngeal carcinoma. The tumor shows a low CD of 4806 cells per square millimeter, 32% nuclear area, 49% stromal area, NC ratio of 1.66, and high ADC of 1.26×10^{-3} mm²/sec.

tumor with dense cellularity. A very strong interdependence between percentage area of nuclei and stroma was seen, which indicates that cellularity and stromal area were indistinguishable and interchangeable. The strong correlation between percentage area of nuclei and stroma might call into question the methodologic independence; however, the two variables were calculated by using the Positive Pixel Count algorithm with different settings. Also, we found NC ratio to have a strong negative correlation with ADC, compared with the percentage area of nuclei. This NC ratio might be interpreted as the amount of cytoplasm per cell. The inverse correlation suggests that tumors with high NC ratio are likely to have densely packed cells with only a limited amount of cytoplasm, reflected by a low ADC.

Several studies have been conducted to investigate the prognostic value of ADC for determination of pretherapeutic tumor radiosensitivity, and a high ADC was reported to be predictive for local nonresponders (8,9). It is often hypothesized that this is due to necrotic parts within the tumor. Our study is the first to prove that low CD reflects a large stromal area that contributes to relatively high ADC values. Stromal component has shown to be an independent prognostic factor for a relapse-free period in several tumors, such as breast cancer, colon cancer, and esophageal squamous cell carcinoma (23–27). Furthermore, it has been described that stromal cells play an important role in the support of tumor growth by promoting invasion and protection from apoptosis and potentially creating barriers to deliver systemic chemotherapy (28–30). This might suggest that the poor prognostic value of a high pretreatment ADC might be partly attributed to the tumor-stromal component. In our study, we found no significant association between histologic tumor grade and mean ADC, although a trend was observed toward lower ADC values in poorly differentiated tumors compared with moderately differentiated tumors. The small sample size and the small variety in differentiation grade hamper the acquisition of significant results. However, a similar trend was reported recently (31). In addition, all tumors showed less than 5% necrosis. Therefore, necrosis was not excluded or treated as a separate parameter.

Our study had several limitations. One limitation of this work was that the DWI was affected by anterior-posterior geometrical distortions. To overcome this, the tumor was manually delineated on the DWI sections on the corresponding craniocaudal level. Clearly, a nonrigid registration method would have been preferable, enabling a voxel-based analysis that included analysis of tissue surrounding the tumor. The color-based segmentation and the usage of identical settings for all patients served to remove a large element of subjectivity and potential bias. The drawback of this method is that staining variability is not taken into account. For the absolute number of cells, we used an automatic segmentation technique with a 9.6% bias and a standard deviation of 11.4%, which we considered acceptable. This introduces some uncertainty in our data. Another limitation was that the number of

Figure 5

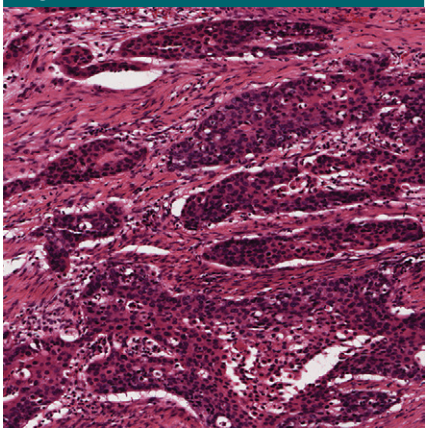

Figure 5: Digitized whole-mount H-E section (original magnification, ×10) of a T3 hypopharyngeal carcinoma. The tumor shows an intermediate CD of 6188 cells per square millimeter, 38% nuclear area, 38% stromal area, NC ratio of 1.59, and intermediate ADC of 1.19 × 10^{-3} mm^2/sec.

Figure 6

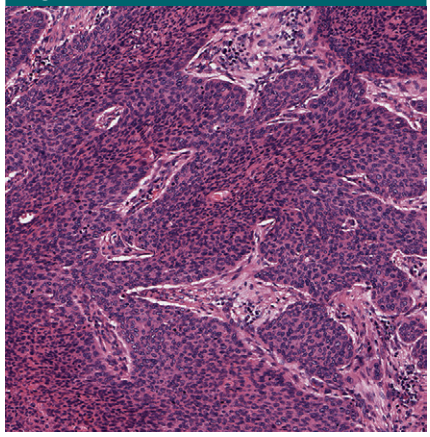

Figure 6: Digitized whole-mount H-E section (original magnification, ×10) of a T4a laryngeal carcinoma. The tumor shows a high CD of 8050 cells per square millimeter, 65% nuclear area, 18% stromal area, NC ratio of 4.14, and low ADC of 0.96 × 10^{-3} mm^2/sec.

patients was small, especially for the color-based segmentation, where four patients had to be excluded because of poor staining intensity. Still, even with this limited number of patients, we found significant correlations between ADC and tissue components.

In conclusion, individual tissue components in laryngeal and hypopharyngeal squamous cell carcinomas significantly affected ADC. ADC inversely correlated with CD, nuclear area, and NC ratio and positively correlated with stromal area. Additionally, nuclear and stromal areas showed strong interdependence. These results give us insights into how ADC reflects the underlying microenvironment of laryngeal and hypopharyngeal cancers. The positive correlation of ADC and stromal component suggests that the poor prognostic value of high pretreatment ADC might partly be attributed to the tumor-stroma component, a known predictor of local failure.

Acknowledgment: The authors thank Dr S. Willems, from the Department of Pathology, for his special help during the revision of this manuscript.

Disclosures of Conflicts of Interest: J.P.D. No relevant conflicts of interest to disclose. **J.C.M.** No relevant conflicts of interest to disclose. **L.M.J.** No relevant conflicts of interest to disclose. **F.A.P.** No relevant conflicts of interest to disclose. **N.K.** No relevant conflicts of interest to disclose. **C.H.J.T.** No relevant conflicts of interest to disclose. **W.G.** No relevant conflicts of interest to disclose. **M.E.P.P.** No relevant conflicts of interest to disclose.

References

1. Padhani AR. Diffusion magnetic resonance imaging in cancer patient management. Semin Radiat Oncol 2011;21(2):119–140.
2. Koh DM, Padhani AR. Diffusion-weighted MRI: a new functional clinical technique for tumour imaging. Br J Radiol 2006;79(944):633–635.
3. Koh DM, Collins DJ. Diffusion-weighted MRI in the body: applications and challenges in oncology. AJR Am J Roentgenol 2007;188(6):1622–1635.
4. Thoeny HC. Diffusion-weighted MRI in head and neck radiology: applications in oncology. Cancer Imaging 2011;10:209–214.
5. Srinivasan A, Dvorak R, Perni K, Rohrer S, Mukherji SK. Differentiation of benign and malignant pathology in the head and neck using 3T apparent diffusion coefficient values: early experience. AJNR Am J Neuroradiol 2008;29(1):40–44.
6. Vandecaveye V, De Keyzer F, Vander Poorten V, et al. Head and neck squamous cell carcinoma: value of diffusion-weighted MR imaging for nodal staging. Radiology 2009;251(1):134–146.
7. Wang J, Takashima S, Takayama F, et al. Head and neck lesions: characterization with diffusion-weighted echo-planar MR imaging. Radiology 2001;220(3):621–630.
8. Hatakenaka M, Nakamura K, Yabuuchi H, et al. Pretreatment apparent diffusion coefficient of the primary lesion correlates with local failure in head-and-neck cancer treated with chemoradiotherapy or radiotherapy. Int J Radiat Oncol Biol Phys 2011;81(2):339–345.
9. Thoeny HC, Ross BD. Predicting and monitoring cancer treatment response with diffusion-weighted MRI. J Magn Reson Imaging 2010;32(1):2–16.
10. Vandecaveye V, Dirix P, De Keyzer F, et al. Predictive value of diffusion-weighted magnetic resonance imaging during chemoradiotherapy for head and neck squamous cell carcinoma. Eur Radiol 2010;20(7):1703–1714.
11. Hatakenaka M, Shioyama Y, Nakamura K, et al. Apparent diffusion coefficient calculated with relatively high b-values correlates with local failure of head and neck squamous cell carcinoma treated with radiotherapy. AJNR Am J Neuroradiol 2011;32(10):1904–1910.
12. Lambrecht M, Vandecaveye V, De Keyzer F, et al. Value of diffusion-weighted magnetic resonance imaging for prediction and early assessment of response to neoadjuvant radiochemotherapy in rectal cancer: preliminary results. Int J Radiat Oncol Biol Phys 2012;82(2):863–870.
13. Vandecaveye V, Dirix P, De Keyzer F, et al. Diffusion-weighted magnetic resonance imaging early after chemoradiotherapy to monitor treatment response in head-and-neck squamous cell carcinoma. Int J Radiat Oncol Biol Phys 2012;82(3):1098–1107.
14. Lambrecht M, Dirix P, Vandecaveye V, De Keyzer F, Hermans R, Nuyts S. Role and value of diffusion-weighted MRI in the radiotherapeutic management of head and neck cancer. Expert Rev Anticancer Ther 2010;10(9):1451–1459.
15. Barajas RF Jr, Rubenstein JL, Chang JS, Hwang J, Cha S. Diffusion-weighted MR imaging derived apparent diffusion coefficient is predictive of clinical outcome in primary central nervous system lymphoma. AJNR Am J Neuroradiol 2010;31(1):60–66.
16. Gibbs P, Liney GP, Pickles MD, Zelhof B, Rodrigues G, Turnbull LW. Correlation of ADC and T2 measurements with cell density in prostate cancer at 3.0 Tesla. Invest Radiol 2009;44(9):572–576.
17. Zelhof B, Pickles M, Liney G, et al. Correlation of diffusion-weighted magnetic reso-

nance data with cellularity in prostate cancer. BJU Int 2009;103(7):883–888.

18. Wang XZ, Wang B, Gao ZQ, et al. Diffusion-weighted imaging of prostate cancer: correlation between apparent diffusion coefficient values and tumor proliferation. J Magn Reson Imaging 2009;29(6):1360–1366.
19. Langer DL, van der Kwast TH, Evans AJ, et al. Prostate tissue composition and MR measurements: investigating the relationships between ADC, T2, K(trans), v(e), and corresponding histologic features. Radiology 2010;255(2):485–494.
20. Ichikawa Y, Sumi M, Sasaki M, Sumi T, Nakamura T. Efficacy of diffusion-weighted imaging for the differentiation between lymphomas and carcinomas of the nasopharynx and oropharynx: correlations of apparent diffusion coefficients and histologic features. AJNR Am J Neuroradiol 2012;33(4):761–766.
21. Caldas-Magalhaes J, Kasperts N, Kooij N, et al. Validation of imaging with pathology in laryngeal cancer: accuracy of the registration methodology. Int J Radiat Oncol Biol Phys 2012;82(2):e289–e298.
22. Borren A, Moman MR, Groenendaal G et al. Why prostate tumour delineation based on apparent diffusion coefficient is challenging: an exploration of the tissue microanatomy. Acta Oncol 2013;52(8):1629–1636.
23. Wang K, Ma W, Wang J, et al. Tumor-stroma ratio is an independent predictor for survival in esophageal squamous cell carcinoma. J Thorac Oncol 2012;7(9):1457–1461.
24. de Kruijf EM, van Nes JG, van de Velde CJ, et al. Tumor-stroma ratio in the primary tumor is a prognostic factor in early breast cancer patients, especially in triple-negative carcinoma patients. Breast Cancer Res Treat 2011;125(3):687–696.
25. Huijbers A, Tollenaar RA, v Pelt GW, et al. The proportion of tumor-stroma as a strong prognosticator for stage II and III colon cancer patients: validation in the VICTOR trial. Ann Oncol 2013;24(1):179–185.
26. Wiseman BS, Werb Z. Stromal effects on mammary gland development and breast cancer. Science 2002;296(5570):1046–1049.
27. Mesker WE, Liefers GJ, Junggeburt JM, et al. Presence of a high amount of stroma and downregulation of SMAD4 predict for worse survival for stage I-II colon cancer patients. Cell Oncol 2009;31(3):169–178.
28. Koontongkaew S. The tumor microenvironment contribution to development, growth, invasion and metastasis of head and neck squamous cell carcinomas. J Cancer 2013;4(1):66–83.
29. Neesse A, Michl P, Frese KK, et al. Stromal biology and therapy in pancreatic cancer. Gut 2011;60(6):861–868.
30. Mueller MM, Fusenig NE. Friends or foes—bipolar effects of the tumour stroma in cancer. Nat Rev Cancer 2004;4(11):839–849.
31. Varoquaux A, Rager O, Lovblad KO, et al. Functional imaging of head and neck squamous cell carcinoma with diffusion-weighted MRI and FDG PET/CT: quantitative analysis of ADC and SUV. Eur J Nucl Med Mol Imaging 2013;40(6):842–852.